Original Research Article

The acoustic performance of a dual Helmholtz resonators system in the presence of a grazing flow

Rong Xue [a], Cheuk Ming Mak [a,] *, Dizi Wu [b], Kuen Wai Ma [a]

[a] *Department of Building Environment and Energy Engineering, The Hong Kong Polytechnic University, Hung Hom, Kowloon, Hong Kong*

[b] *School of Architecture, Changsha University of Science & Technology, Changsha, Hunan, China*

*Corresponding author.
E-mail Address: cheuk-ming.mak@polyu.edu.hk (C.M.Mak).
Telephone: +852 2766 5856
Fax: +852 2765 7198

Abstract

Helmholtz resonators (HR) are widely used in aero-engine systems for noise reduction. By connecting a pair of HRs in series (neck-cavity-neck-cavity), a dual HRs system is formed. This study investigated the influence of neck length, cavity volume and flow Mach number on the noise attenuation performance of a dual HRs system. A three-dimensional numerical simulation was performed to calculate the transmission loss results. The transmission loss (TL) results indicated that the second neck length can influence the second resonance frequency and $TL_{max.}$ Changing the cavity volume significantly influences the noise attenuation ability under lower flow rate conditions compared to higher flow rate conditions. The flow Mach number had a more significant impact on the first TL peak than on the second TL peak. This study shows the relationship between the geometric parameters, grazing flow and noise attenuation performance of a dual HRs system and could provide guidance in designing suitable dual HRs for aero-engine systems.

Keywords: Helmholtz resonator; transmission loss; noise attenuation; aeroacoustics; grazing flow.

1. Introduction

Aircraft noise pollution significantly affects human life and causes stress-mediated health effects [1-3]. There are two primary sources of aircraft noise: aerodynamics and engine. Engines can generate strong noises when they are working[4, 5], and an acoustic absorber can effectively reduce aero-engine noise. Various studies have focused on designing high-performance aero-engine mufflers.

A Helmholtz resonator (HR) is a common muffler used to reduce acoustic noise in aircraft engines and exhaust systems. Several engineers and researchers have been engaged in designing HR with high noise-reduction ability. Ingard[6] studied the influence of different orifice geometries on the resonant frequency of HR. Chanaud[7] summarized a theoretical equation to calculate the shift in the resonant frequency due to changes in the shape of the neck. Selamet *et al.* [8] used the boundary element method (BEM) to numerically predict the resonant frequency of the HR. They also investigated the noise attenuation ability with different cavity dimensions. Selamet and Lee[9] extended the inner neck length of the HR to improve the sound attenuation ability in a small place. Shi and Mak[10] used the transfer matrix method to predict the noise attenuation ability of the HR with a spiral neck. Cai *et al.*[11] compared the above-mentioned configurations theoretically and numerically. The results of their study showed that a good design of the Helmholtz resonator could effectively attenuate the acoustic wave more in constrained spaces. VanDercreek *et al.*[12, 13] investigated the aeroacoustics performance of different cavity geometries by using the acoustic imaging method.

Aircraft engines and exhaust systems are always accompanied by a grazing flow. When a HR is exposed to flow, a strong flow fluctuation is produced[14]. The convection of the unsteady vortex shedding emerged near the neck of the HR[15]. The flow behavior influences the noise attenuation ability. Kim and Selamet [16] investigated the noise attenuation performance of a HR under different flow Mach numbers experimentally. The results of their study indicated that

the flow could shift the resonant frequency to a higher frequency domain and reduce the peak magnitude of transmission loss (TL_{max}). This finding was numerically confirmed by Wu *et al.* [17]. Researchers have proposed different implementation configurations of HRs to improve noise attenuation ability under grazing flow. Dastourani *et al.* [18] investigated the effect of grazing flow Mach numbers and discussed the influence of the cavity shapes on the noise attenuation ability of the HR. By increasing the flow Mach numbers, the TL_{max} decreases significantly. In addition, the resonance frequency was reduced 30% by changing the HR cavity shape from sphere to cubic. Zhao *et al.* [19] conducted numerical research to investigate the effects of the extended neck on HR under a grazing flow. The results of their study demonstrated that the extended neck can increase 5-11dB transmission loss at a higher Mach number. Pan *et al.* [20]studied the transmission loss ability of two coupled HRs with a sharable sidewall. The numerical results showed that the coupled HRs could provide multiple transmission loss peaks. In addition, the perforated orifice in the sharable sidewall strongly influenced TL_{max}.

The dual HRs system was first introduced by Xu *et al.* [21]. This type of HRs system includes a pair of necks and cavities connected in series (neck-cavity-neck-cavity). Cai *et al.* [22] compared the acoustic characteristics of different HRs array configurations theoretically and numerically. The results showed that dual HRs could provide two resonance frequencies and increase the broadband noise reduction ability. Kim and Selamet [23] performed an experiment to measure the transmission loss and acoustic impedance of a dual HR under a grazing flow. The results indicated that both TL_{max} values decreased as the flow Mach number increased, and the resonance frequencies tended to move to higher frequencies. In practical engines, dual HRs can utilize the constrained space and provide two resonance frequencies, indicating that it can be an effective silencer in aero-engines. However, the relationship between the transmission loss performance of the dual HRs system and the geometric parameters, particularly the second

neck and cavity, remain unclear. It can be seen that these results could assist in optimizing aero-engine mufflers.

In this study, a numerical study was conducted to discuss the noise attenuation ability of a dual HRs system under different flow Mach numbers. In Section 2, the numerical method and the simulation strategy were explained. In Section 3, the results were compared with the existing experimental results to validate the correctness of the numerical methods. Subsequently, the effects of the second neck length, cavity volume, and flow Mach number were examined. Finally, Section 4 summarized the key findings and conclusions.

2. Numerical model and simulation strategy

2.1 Numerical Model

This study used the commercial numerical software COMSOL Multiphysics to numerically investigate the noise attenuation ability and flow distribution of the HR. The numerical method was consisted of three steps[18]: first, a computational fluid dynamics (CFD) simulation was employed to solve the background flow under a very fine mesh; then, the turbulent results were mapped to a course mesh. Finally, the acoustic results were solved using a coarse mesh. A detailed numerical strategy is presented in this section.

CFD Module

The Reynolds averaged Navier–Stokes (RANS) model was widely used to simulate the background flow of the HR. Researchers have used the RANS model to simulate the flow inside ductwork systems and the HRs[17, 19, 20]. The numerical results showed that RANS Model is capable of capturing the time-averaged flow and vortex in the ductwork system. Researchers have also used the Large Eddy Simulation (LES) model to capture the time-dependent vortex-acoustic coupling behavior of the HR[14, 24]. In this study, the RANS model is sufficient to simulate the background flow, and it could save computing resources. For a compressible, steady-state airflow, the governing equations are as follows:

$$\nabla \cdot (\rho \mathbf{u}) = 0 \tag{1}$$

$$\rho(\mathbf{u} \cdot \nabla)\mathbf{u} = \nabla \cdot [\mu(\nabla \mathbf{u} + (\nabla \mathbf{u})^T) - p\mathbf{I} - \frac{2}{3}\mu(\nabla \cdot \mathbf{u})\mathbf{I}] + \mathbf{F} \tag{2}$$

where ρ denotes the air density, $\mathbf{u}$ is velocity, $\mathbf{I}$ is the identity matrix, μ is the dynamic viscosity coefficient, and $\mathbf{F}$ is the source term.

The *k-ε* turbulence model has been widely used to simulate the flow inside a ductwork system. Therefore, this model was chosen for the present study. The turbulence kinetic energy (*k)* and the rate of dissipation of the turbulence kinetic energy (*ε)* must be solved using the following equations:

$$\rho(\mathbf{u} \cdot \nabla)k = \nabla \cdot ((\mu + \frac{\mu_T}{\sigma_k})\nabla k) + P_k - \rho\varepsilon \tag{3}$$

$$\rho(\mathbf{u} \cdot \nabla)\varepsilon = \nabla \cdot ((\mu + \frac{\mu_T}{\sigma_\varepsilon})\nabla \varepsilon) + C_{\varepsilon 1}\frac{\varepsilon}{k}P_k - C_{\varepsilon 2}\frac{\varepsilon^2}{k}\rho \tag{4}$$

where σ_k, σ_ε, $C_{\varepsilon 1}$ and $C_{\varepsilon 2}$ are constants, μ_T is the turbulent viscosity, P_k is the production term.

Mapping Between CFD and Acoustics Mesh

In this study, two different meshes were built to separately calculate the CFD results and acoustic responses. Therefore, a mapping study must be used to map and smooth the background flow of CFD variables onto the acoustics mesh by solving an additional set of equations. The mapping strategy is achieved by solving:

$$P_{0,aco} - P_0 = \delta h^2 \nabla \cdot (\nabla P_{0,aco}) \tag{5}$$

$$\mathbf{u}_{0,aco} - \mathbf{u}_0 = \delta h^2 \nabla \cdot (\nabla \mathbf{u}_{0,aco}) \tag{6}$$

$$\rho_{0,aco} - \rho_0 = \delta h^2 \nabla \cdot (\nabla \rho_{0,aco}) \tag{7}$$

$$T_{0,aco} - T_0 = \delta h^2 \nabla \cdot (\nabla T_{0,aco}) \tag{8}$$

$$\mu_{T,aco} - \mu_T = \delta h^2 \nabla \cdot (\nabla \mu_{T,aco}) \tag{9}$$

where P_0, $\mathbf{u}_0$, ρ_0, T_0 and μ_T are the mean background flow pressure, velocity, density, temperature and turbulent viscosity, respectively; $P_{0,aco}$, $\mathbf{u}_{0,aco}$ $\rho_{0,aco}$ $T_{0,aco}$ and $\mu_{T,aco}$ are these parameters mapped onto the acoustic mesh. δ is constant and h is the mesh size.

Acoustic Module

The linearized Navier-Stokes, frequency domain (LNSF) interface of the COMSOL Multiphysics was used to calculate the acoustic response of HR. The governing equations are given as follows:

$$\rho_0(i\omega\mathbf{u}_t+(\mathbf{u}_t\cdot\nabla)\mathbf{u}_0+(\mathbf{u}_0\cdot\nabla)\mathbf{u}_t)+\rho_t(\mathbf{u}_0\cdot\nabla)\mathbf{u}_0=\nabla\cdot\boldsymbol{\sigma}+F-\mathbf{u}_0M \quad (10)$$

$$i\omega\rho_t+\nabla\cdot(\rho_0\mathbf{u}_t+\rho_t\mathbf{u}_0)=M \quad (11)$$

$$\rho_0C_p(i\omega T_t+\mathbf{u}_t\cdot\nabla T_0+\mathbf{u}_0\cdot\nabla T_t)+\rho_tC_p(\mathbf{u}_0\cdot\nabla T_t)-\alpha_pT_0(i\omega p_t+\mathbf{u}_t\cdot\nabla p_0+\mathbf{u}_0\cdot\nabla p_t)-\alpha_pT_t(\mathbf{u}_0\cdot\nabla p_t)=\nabla\cdot(k\nabla T_t)+\Phi+Q \quad (12)$$

where $\mathbf{u}_t$, p_t, T_t and ρ_t are the acoustic perturbations of velocity, pressure, temperature and density, respectively. The right-hand terms, *M*, ***F*** and *Q* are the source terms. C_p is the heat capacity. $\boldsymbol{\sigma}$ is the stress tensor and Φ is the viscous dissipation function.

2.2 Description of the simulation strategy

Geometric dimensions

As shown in Fig.1, the geometry includes a dual HRs array attached to one side of the rectangular main duct. The influence of the actual flight conditions of the engines was ignored in this study. The dual HRs include two necks and two cavities, and these parts are connected in series. The volumes of the two cavities are *V1* and *V2*. The lengths of the two necks are *Ln1* and *Ln2*. In this study, the effect of neck length and cavity volumes were discussed. The lengths of the neck were changed from 0cm to 7.62cm (0in to 3in), and the cavity volumes were changed from 926.3 cm^3 to 1852.6 cm^3. The flow Mach numbers, *Ma*, were varied from 0 to 0.12. The geometrical dimensions and the flow conditions of the dual HRs system are summarized in Table 1.

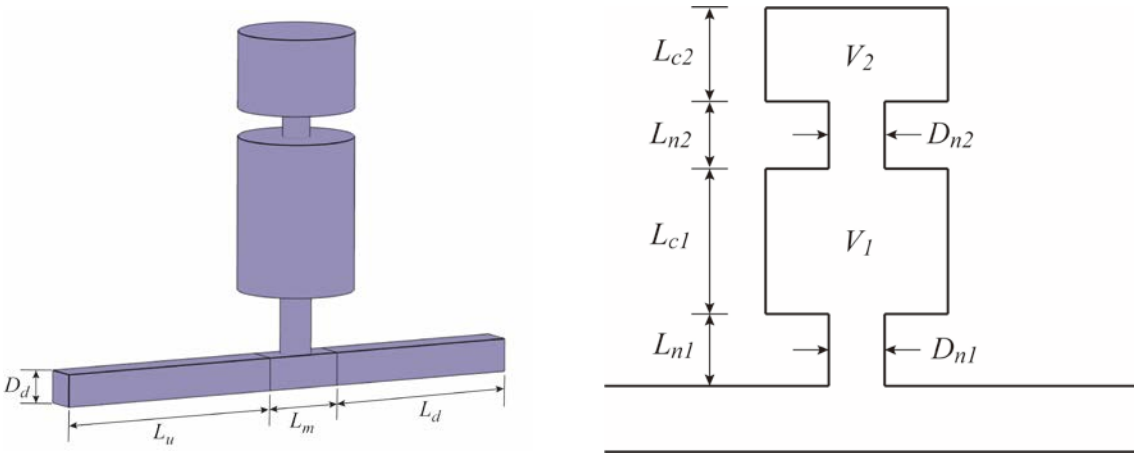

(a) (b))

Fig.1. Schemes of a dual HRs system.

Table 1. Geometric parameters and flow conditions of the dual HRs system.

Parameters	Values	Parameters	Values
D_d	4.3cm	*Dn2*	3.5cm
Lu	25 cm	*V1,V2*	926.3-1852.6cm^3
Lm	10 cm	*f*	1-1000Hz
Ld	30 cm	*P0*	101.325kPa
Ln1	8.5 cm	*c*	343m/s
Lc1,Lc2	10.16-20.32 cm	*Ma*	0-0.12
Ln2	0-7.62 cm	*ρ0*	1.2kg/m3
Dn1	4 cm	*T0*	293.15K

Boundary Conditions

By considering the symmetry of the geometry model, numerical simulations were performed for half of the dual HRs model. For CFD simulations, the inlet and outlet were set as the fully developed flow inlet and pressure outlet, respectively. The boundaries of the dual HRs and main duct were set as no-slip walls. For the acoustic simulations, the upstream and downstream were set as a perfectly matched layer (PML) to reduce the reflected acoustic wave. Behind the upstream PML, a background acoustic wave is generated in a small region. The boundaries of the acoustic simulations were set as slip wall and adiabatic conditions. Fig.2 shows the detailed boundary conditions.

(a) (b)

Fig.2. Boundary condition of the simulation models. (a) CFD module; (b) acoustic model.

Computational Mesh

As shown in Fig.3, two different meshes were used to simulate the flow and acoustic field. To capture the turbulence accurately, it is necessary to refine the specific areas of the computational domain. Fig.3(a) shows the mesh refinement near the boundary layer, resonator neck, and junction area between the resonator and main duct. A swept mesh was used to reduce the computational resources near the upstream and downstream regions of the main duct. Fig.3(b) shows the computational mesh for the acoustic simulation. Swept meshes were used in the PML region. The other parts used an unstructured tetrahedral mesh.

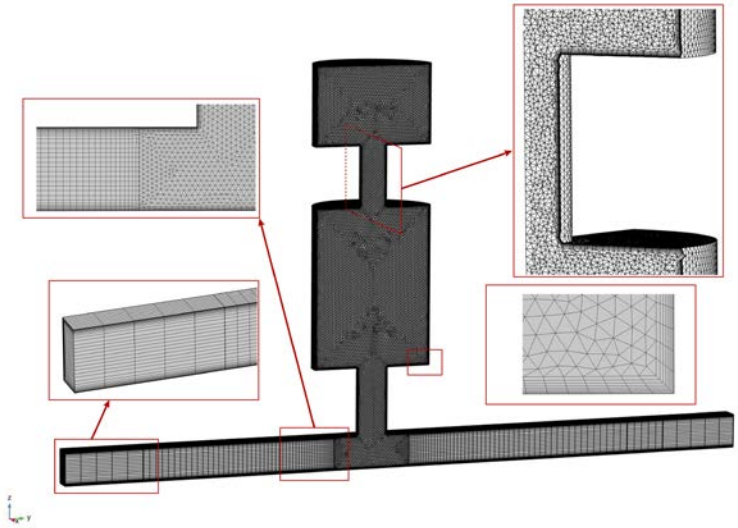

(a)

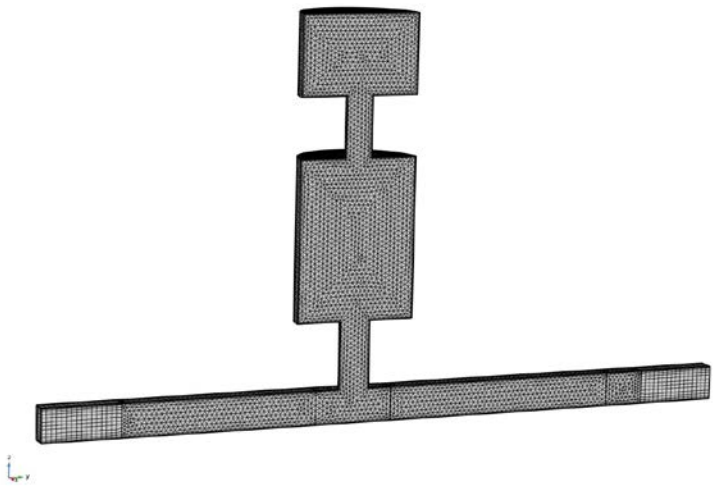

(b)

Fig.3. Schematics of meshes distribution. (a) mesh for CFD simulation with details of the inlet, boundary layer, resonator neck and the junction area between the resonator and main duct; (b) Mesh for acoustic simulation.

In this section, a grid convergence study was performed to select a suitable mesh to finish the CFD simulation. As shown in Fig.4, four sets of meshes were used to calculate the velocity distribution near the neck inlet along the x-axis. The numbers of grids were 662229 (mesh1), 753,394 (Mesh2), 874,094 (mesh3), and 1,271,660 (mesh4). Finally, Mesh3 was chosen for CFD simulation. The total number of CFD grids was 874,094. The total number of acoustic grids was 284,937.

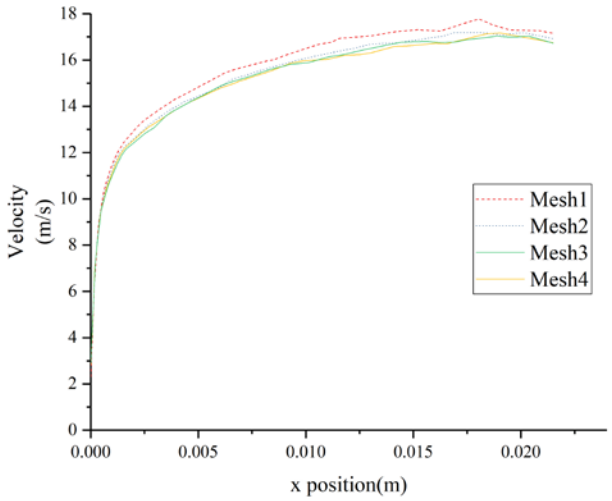

Fig.4. grid convergence verification.

3. Results and Discussion

3.1 Numerical validation

The numerical results were compared with the experiments performed by Kim and Selamet [23] to examine the accuracy of the acoustic simulation method. All geometric dimensions in this simulation were set the same as the experimental measurement. The flow Mach numbers (0,0.05 and 0.1) were also the same as the experimental conditions. The frequency range was chosen as 1-300Hz. Fig 5 shows the transmission loss results of the dual HRs system at different flow Mach numbers. The experiment results were obtained by Kim and Selamet[23]. The transmission loss is defined as:

$$TL = 20\log_{10}(|\frac{P_{in}}{P_{out}}|) \tag{13}$$

where P_{in} is the pressure amplitude of the incident acoustic waves on the upstream main duct, and P_{out} is the amplitude of the transmitted acoustic waves on the downstream main duct. It can be seen that our numerical results match the experimental results well, which means that the simulation model has relatively high accuracy.

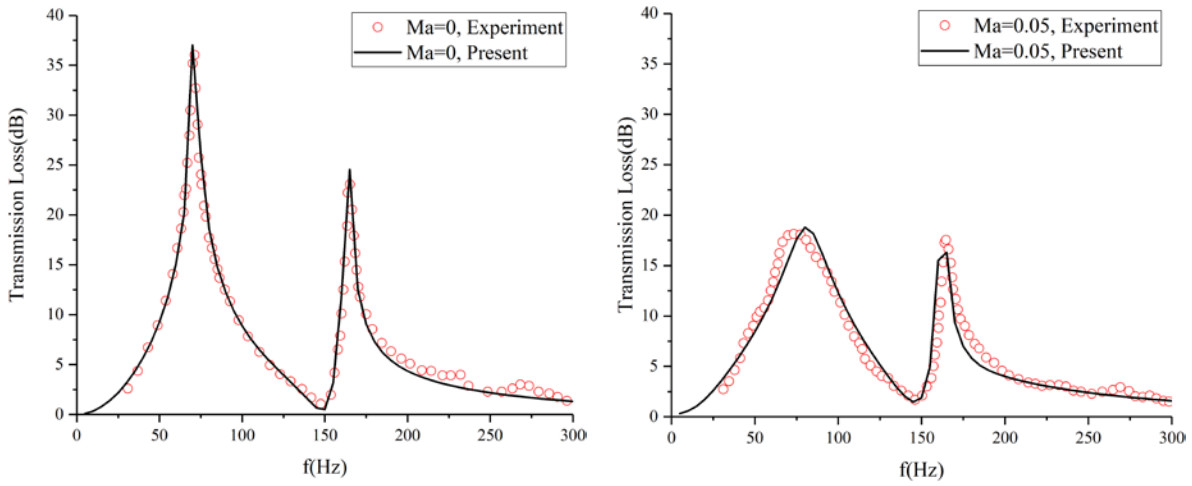

(a) (b)

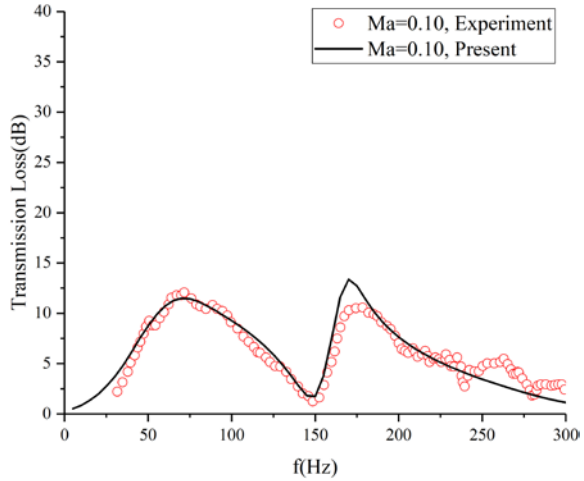

(c)

Fig. 5. Comparison of the TL results between existing experiments[23] and present simulations (a) *Ma*=0; (b)*Ma* =0.05; (c) *Ma* =0.1. Black lines and red dots represent the experiment and numerical results respectively.

To validate the accuracy of the CFD simulation, the velocity profile of the main duct was compared with analytical results. According to the power low, the velocity profile is determined by[25]:

$$V(y^*) = V_{\max}[-4y^*(y^*-1)]^{(1/7)} \tag{14}$$

where y^* is the non-c y position, $V_{\max}$ is the maximum velocity. The main duct velocity profile at 5cm before the dual HRs model was calculated by using equation(14). As shown in Fig.6, when *Ma*=0.05, the time-averaged velocity profile of CFD simulation is consistent with analytical results, which means the flow field of simulation is correct.

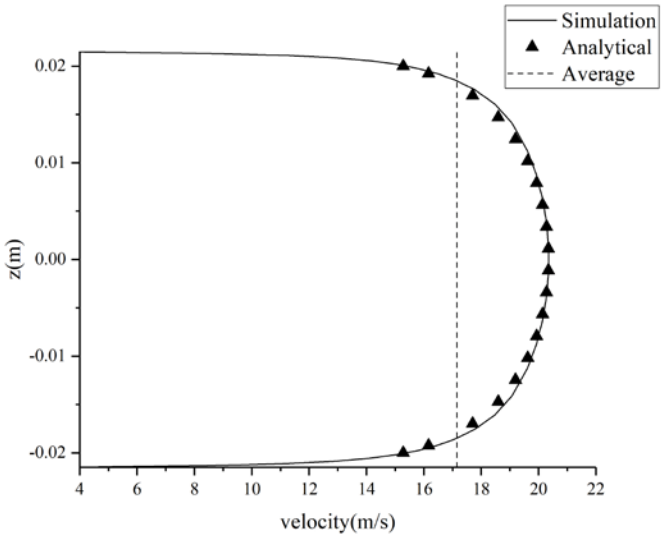

Fig. 6. The velocity profile of simulation (solid line), analytical (symbols) and averaged result (dashed line), *Ma*=0.05.

3.2 Effect of the neck length between two cavities

In this section, the effect of the neck length between the two cavities of the dual HRs system was investigated. A HR can be regarded as a second-order mass-spring system[24], and the mass is fully determined by the neck geometry. Therefore, for a dual HRs system, the neck length between the two cavities can influence the noise attenuation ability. The transmission loss results of different second neck lengths were evaluated and summarized in Fig.7. The flow Mach numbers were selected as 0.05 and 0.1, which are typical flow speeds in the duct system of the aero-engines. Neck lengths were selected as 0in, 0.5in, 1.5in and 3in. The geometric parameters of the main duct and cavity volume were the same as the dual HRs model in Section 3.1.

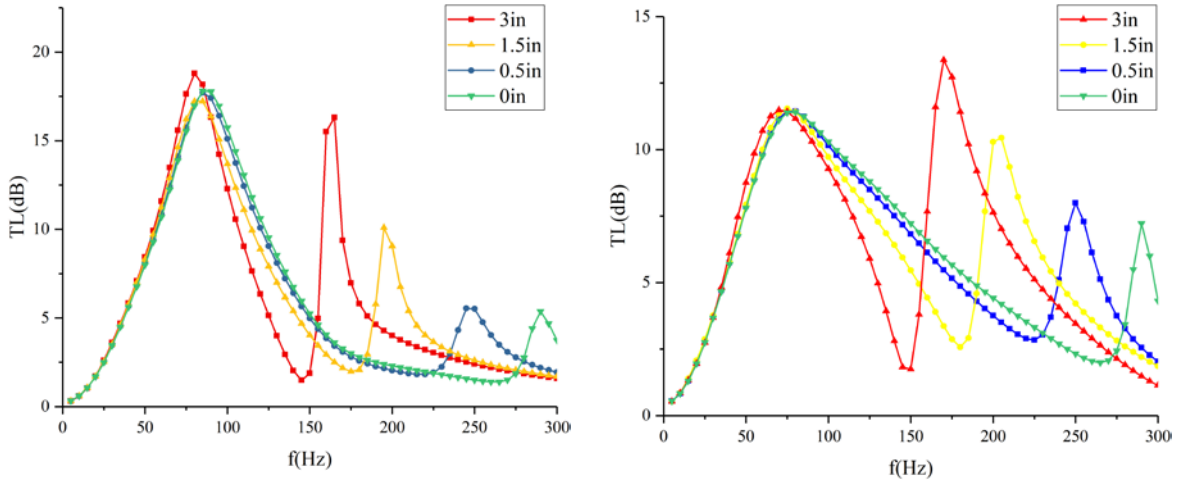

Fig. 7. Transmission loss versus frequency for different neck length values (a) *Ma*=0.05; (b) *Ma*=0.1

For the dual HRs system, two resonant peaks of the transmission loss existed in the frequency domain of 1-300Hz. This finding was confirmed in other studies[21-23]. It can be observed that when the length of the second neck increased, the first resonant frequency remained unchanged, but the second resonant frequency decreased. The maximum transmission loss, TL_{max}, increased as the neck length increased. In particular, with a long neck

length (3in), the second TL_{max} can be greater than the first peak when Ma=0.1. The resonance frequency and TL_{max} for different Mach numbers and neck lengths were summarized in Table 2. For the first TL peak, TL_{max} decreased by nearly 37% when Ma increased from 0.05 to 0.1. However, with a short neck length (0in and 0.5in), the second TL peak increased by a maximum of 3. These results showed that the neck length can effectively influence the noise attenuation ability of dual HRs systems effectively. Specifically, increasing the second neck length can increase the TL performance, and a short neck length can increase the TL performance under higher flow rate.

The resonance frequency of a HR can be determined by[22]:

$$\omega_0 = c_0\sqrt{\frac{S_n}{l_n V_c}} \tag{15}$$

where ω_0 is the resonance frequency, S_n is the cross-sectional area of the neck, l_n is neck length, V_c is the cavity volume. In this study, the dual HRs have two resonance frequencies. Each resonance frequency is decided by the geometric parameters of each neck and cavity volume. According to equation (15), the second resonance frequency was decreased when the second neck length increased. Besides, the geometric parameters of the first neck remained unchanged. Hence, the first resonance frequency was kept the same in fig.7.

Table 2. The resonance frequency and the maximum transmission loss for different Mach numbers and neck lengths.

		Peak1		Peak2	
		Frequency	TL(dB)	Frequency	TL(dB)
Ma=0.05	0in	85	17.81	290	5.37
	0.5in	85	17.7	245	5.55
	1.5in	85	17.23	195	10.09
	3in	80	18.8	165	16.3
Ma=0.10	0in	80	11.41	290	7.22
	0.5in	75	11.45	250	7.99
	1.5in	75	11.45	205	10.44
	3in	70	11.48	170	13.36

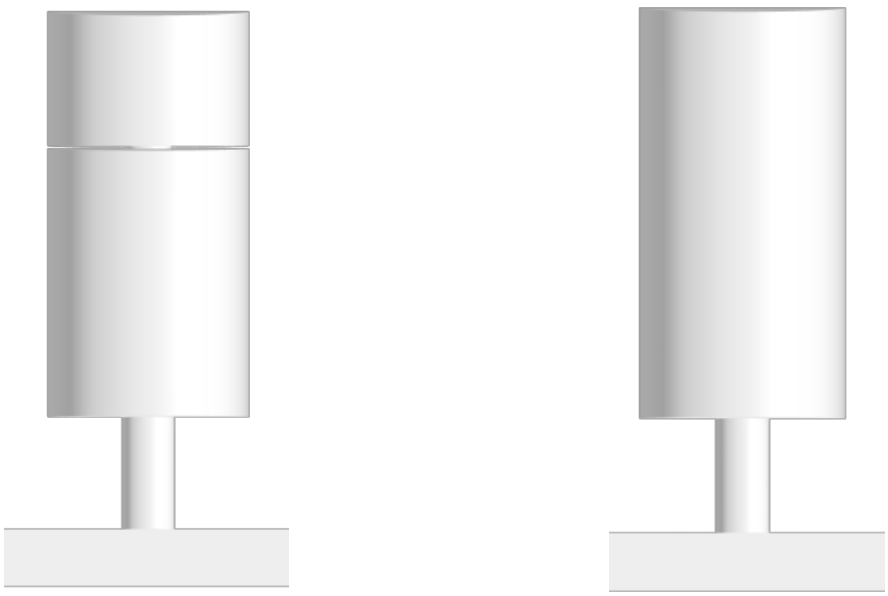

(a) (b)

Fig.8. Schematic of the main duct with a HR system. (a) dual HRs system with neck length *Ln*=0; (b) single HR system.

As shown in Fig.8(a), when the second neck length *Ln2* equals zero, two cavities of the dual HRs system are connected and separated by a perforated wall. If this perforated wall is removed, the dual HRs system can be regarded as a single HR with the same cavity volume (Fig.8(b)). The transmission loss results of these two structures were compared and shown in Fig.9. The thickness of the perforated wall of the dual HRs model used in this study is 2mm, and other geometric parameters are the same as the model in Section 3.1. The cavity volume of the single HR model is 2778.9 cm^3, which is the same as the total volume of the dual HRs model. It can be observed that dual HRs can provide another TL peak than the single HR. For the first TL peak, when *Ma*=0.05, TL_{max} of the single HR was higher than that of the dual HRs. When *Ma*=0.1, the first TL_{max} was nearly the same. Therefore, the noise attenuation ability of dual HRs was better than that of a single HR under higher flow rate conditions.

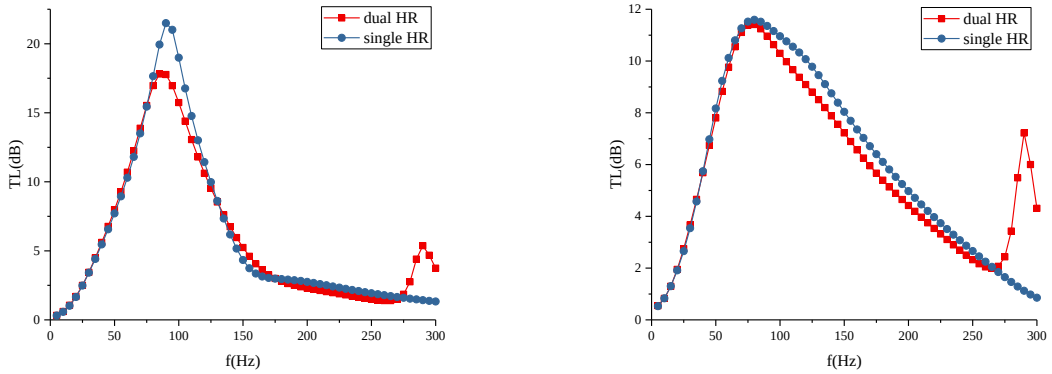

(a) (b)

Fig.9. Comparison of the transmission loss versus frequency for a dual HRs system and a single HR. (a) *Ma*=0.05; (b) *Ma* =0.1

3.3 Effect of the cavity volume

The effect of the cavity volume was investigated and shown in Fig.10. In this study, the total cavity volume of all the dual HRs models was $V1+V2=22778.9\ cm^3$, while the neck length and main duct geometrics were the same as the parameters in Section3.1. Table 3 presents the detailed cavity volumes of each dual HRs system. The effect of the cavity volume was investigated under two different flow velocity conditions: *Ma*=0.05 and *Ma*=0.10. It can be observed that changing the cavity volume influences the resonant peaks and the resonant frequency. When *V2* increased, the second resonant frequency tended to decrease, but the first resonant frequency tended to increase. When *Ma*=0.05, increasing *V2* resulted in a higher second resonant peak. When *Ma*=0.1, resonant peaks were much smaller owing to the high flow rate, and the effect of changing the cavity volume was not obvious. Therefore, adjusting the cavity volume is an effective way to improve the noise attenuation ability under lower flow rate conditions; however, it is, not suitable for a higher flow rate.

In this study, equation (15) can explain the variation of the resonance frequency by changing the cavity volume. From Design1 to Design 3, the first cavity volume *V1* was decreased. According to equation (15), the resonance frequency increase as cavity volume

297 decrease. Therefore, the first resonance frequency was increased from 60Hz to 80Hz when
298 *Ma*=0.05. Besides, it can be observed the variation of the second resonance frequency was also
299 consistent with equation (15).

300 **Table 3.** Characteristics of the dual HRs system with different cavity volume

Dual HRs design	*V1*(cm^3)	*V2*(cm^3)	*V1/V2*
1	1852.6	926.3	2
2	1389.5	1389.5	1
3	926.3	1852.6	0.5

301

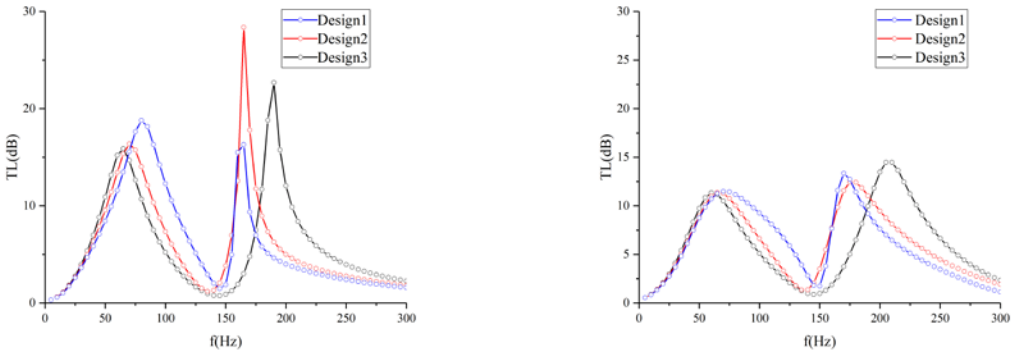

(a) (b)

302 **Fig.10.** Transmission loss results versus frequency for different cavity volume values (a) *Ma*=0.05;
303 (b) *Ma*=0.1

304 Fig.11. shows the flow field results of the dual HRs system with different cavity volumes.
305 The velocity magnitude inside the cavity was converted to a non-dimensional Mach number
306 ($Ma=v/c_0$) to clearly show the velocity distribution. As can be seen in the figure, air entered
307 the first cavity through the downstream side of the neck. As the air entered the cavity, the flow
308 rate decreased gradually. Fig.12 shows the acoustic pressure fields of the dual HRs system
309 under the resonant frequency. The acoustic pressure in the main duct was extremely low due
310 to the resonance occurring. Near the downstream side of the dual HRs system, a secondary
311 acoustic wave source emerged due to the combined effect of grazing flow and acoustic wave.
312 This phenomenon was also mentioned by Dastourani and Bahman-Jahromi[21]. The secondary

acoustic wave source can generate noise. Consequently, the noise attenuation ability of the dual HRs system was reduced owing to grazing flow effect.

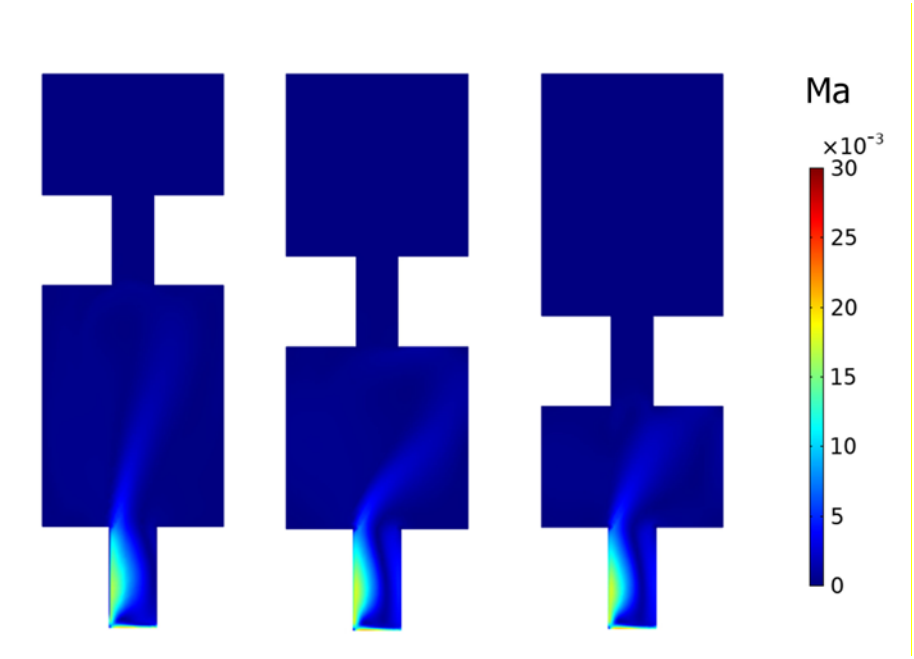

(a)

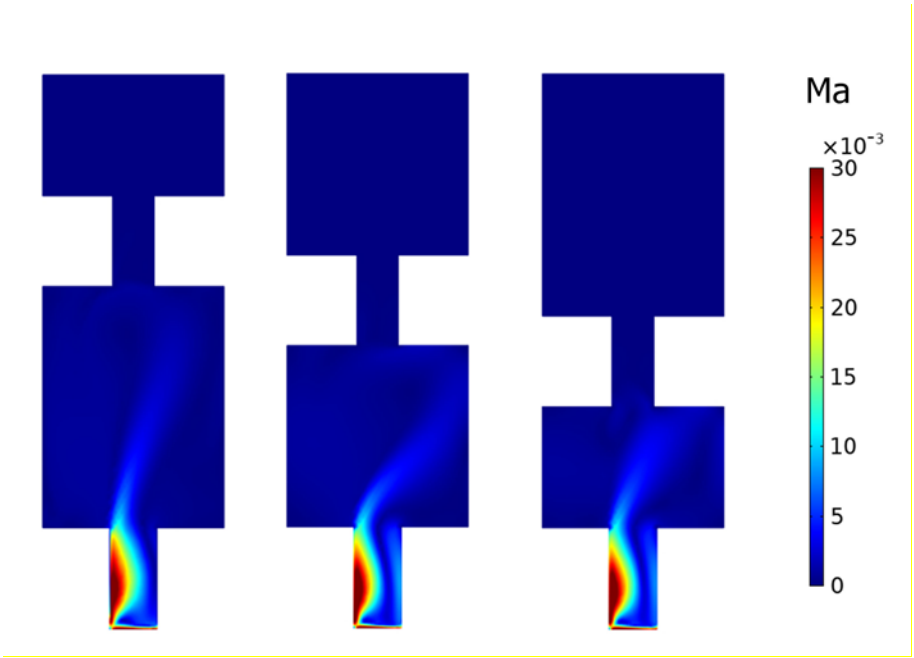

(b)

Fig.11. Velocity fields of dual Helmholtz resonators with different cavity volumes under different Mach numbers (a) *Ma*=0.05; (b) *Ma*=0.1

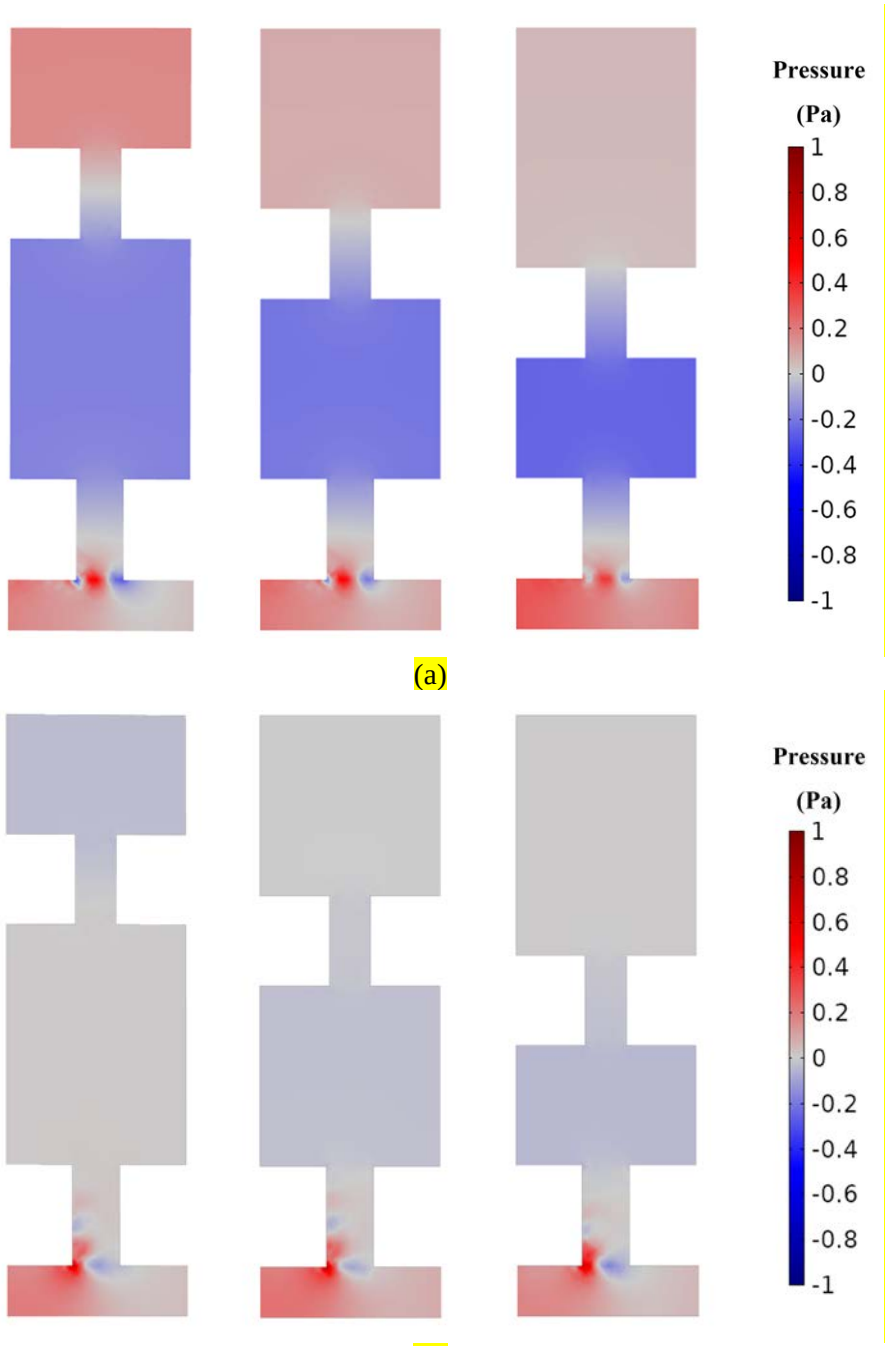

Fig.12. Acoustic pressure fields of dual Helmholtz resonators with different cavity volumes under different Mach numbers (a) *Ma*=0.05; (b) *Ma*=0.1

3.4 Effect of the grazing flow Mach number

In this section, the flow Mach numbers were set as 0, 0.03, 0.05, 0.07, 0.10 and 0.12. The geometric parameters were the same as the dual HRs model used in Section 3.1. The resonance

frequency and the TL_{max} values for different Mach numbers are summarized in Table 4. The effect of the grazing flow Mach number on transmission loss performance is shown in Fig. 13. It can be seen that as *Ma* increased, the first TL_{max} and the second TL_{max} both decreased. The first TL_{max} dropped from 37.0dB to 10.7dB. The second TL_{max} dropped from 24.5dB to 11.0dB. The results indicate that the flow Mach number has a more significant impact on the first TL peak than on the second TL peak. As *Ma* increased, the first resonance frequency increased from 70Hz to 85Hz in the first place, and subsequently dropped back to 70Hz. The second resonance frequency was increased from 165Hz to 170Hz. Zhao *et al.*[19] and Dastourani *et al.*[18] also reported that resonance frequency could not continually increase as *Ma* grows. The resonance frequency of HR is determined by acoustic impedance. According to Kim[23], the acoustic impedance increases when *Ma* grows, leading to a higher resonance frequency. On the other hand, higher *Ma* leads to a higher frequency noise[18], which can decrease the transmission loss performance at the higher frequency domain. The resonance frequency is decided by the above two factors. Therefore, as *Ma* grew, the first resonance frequency increased first and then decreased in our study.

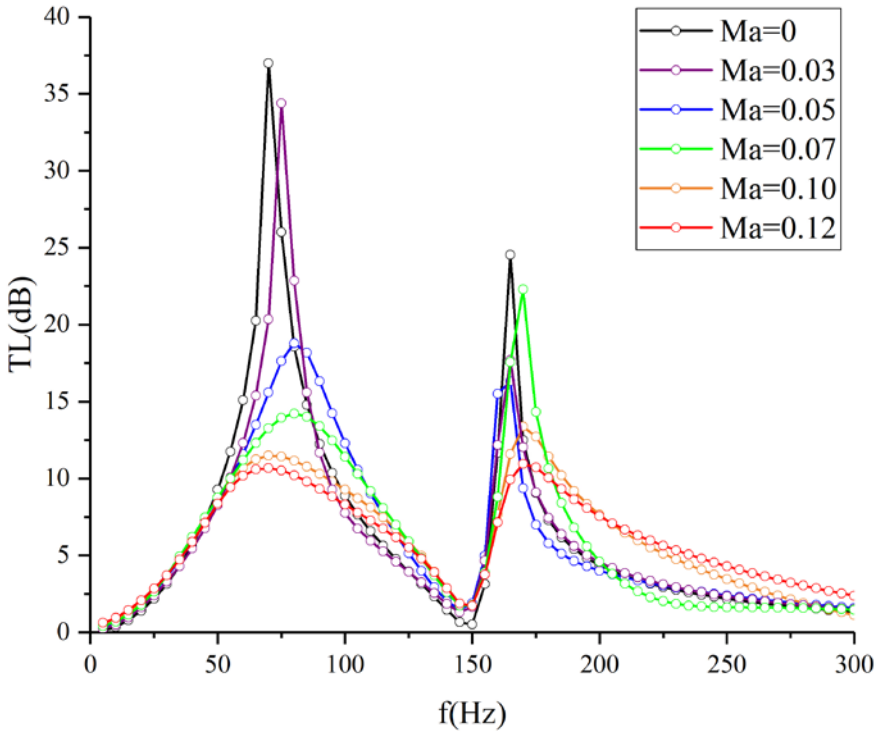

Fig.13. Transmission loss versus frequency for different flow Mach numbers

Table 4. Summary of the resonance frequency and the maximum transmission loss for different Mach numbers

Ma	Peak1		Peak2	
	Frequency	TL(dB)	Frequency	TL(dB)
0	70	37.0	165	24.5
0.03	75	34.4	165	17.7
0.05	80	18.8	165	16.3
0.07	80	14.2	170	22.3
0.10	70	11.5	170	13.4
0.12	70	10.7	170	11.0

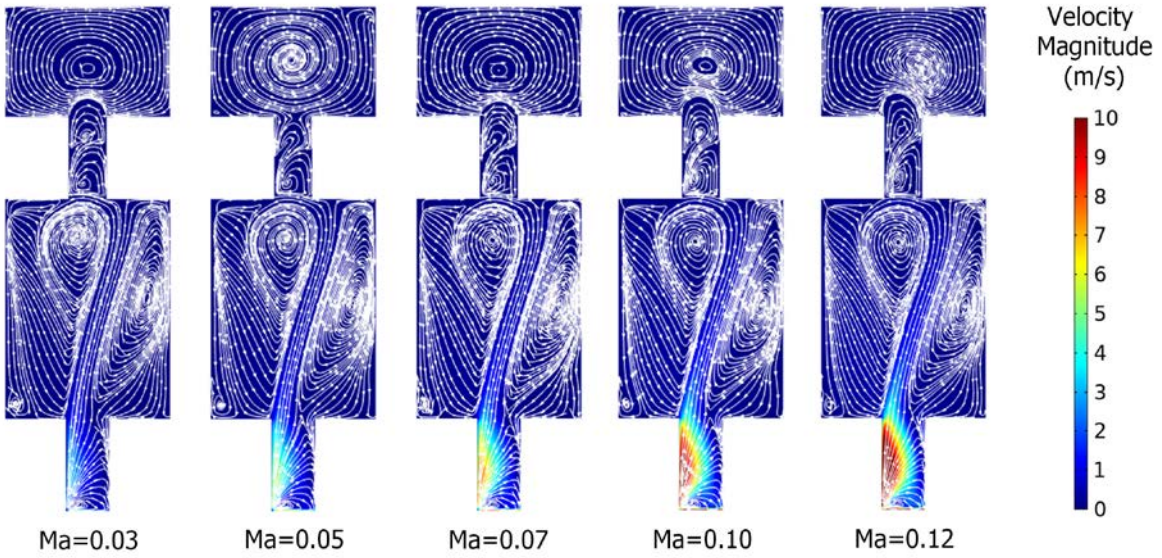

Fig.14. Velocity fields and streamlines of the dual HRs system under different flow Mach numbers

Fig.14 shows the velocity magnitude and streamlines of the dual HRs system under different flow rates. As can be seen from the streamlines, the flow entered the first cavity through the left side of the first neck. Afterward, the streamlines inside the first cavity indicated two vortex centroids emerged. One of the vortices was located just below the second neck and was rotating anti-clockwise; the other vortex was located near the center of the cavity boundary. Air flow near the second neck also generated two vortices rotating in opposite directions. Finally, airflow exited the first cavity from the right side of the cavity. When the flow rate

Mach numbers increased from 0.03 to 0.12, the locations of the vortex centroids remained unchanged. The velocity magnitude indicated that as *Ma* increased, the average velocity in the first cavity increased. The velocity distribution in the first neck and cavity can be identified in the previous studies[17, 18, 26]. However, the velocity magnitude inside the second neck and cavity tended to be zero. The velocity magnitude showed that the first neck was located between a high flow rate region (main duct) and a low flow rate region (first cavity). The velocity difference caused the velocity magnitude inside the first neck can reach nearly 10m/s. On the other hand, the velocity magnitude inside the first cavity and the second cavity was lower compared with the velocity magnitude inside the main duct. Therefore, the velocity magnitude inside the second cavity tended to be zero.

4. Conclusion

In this paper, a numerical analysis was performed to investigate the influence of the geometric parameters and flow Mach number on the noise attenuation ability of the dual HRs system in the presence of grazing flow. The effect of neck length was first investigated. The results indicate that the second resonant frequency and TL_{max} increase with the increasing length of the second neck. Compared with the single HR system, the dual HRs can provide another TL peak and is more suitable as silencers under higher flow rate conditions. Changing the cavity volume will have a significant impact on the resonant frequency and TL_{max} under lower flow rate conditions; however, it is not suitable for a higher flow rate. The acoustic pressure field results demonstrated that a secondary acoustic wave source emerges downstream of the neck. By increasing the grazing flow Mach number, TL_{max} of both peaks decreased, and the second resonance frequency increased. However, the first resonance frequency first increased and then decreased. The transmission loss results indicate that the flow Mach number has a more significant impact on the first TL peak than on the second TL peak. The velocity field results revealed that as *Ma* increased, more air entered the first cavity, and the average

velocity in the first cavity also increased. However, the velocity magnitude inside the second neck and cavity tended to be zero. The relationship between the noise attenuation ability of the dual HRs system and the geometric parameters and flow Mach number could be useful in designing aero-engine mufflers.

Declaration of conflicting interests

The authors declared no potential conflicts of interest with respect to the research, authorship, and/or publication of this article.

Funding

The work described in this article was fully supported by a grant from the Research Grants Council of the Hong Kong Special Administrative Region, China (project 15207820) and the National Natural Science Foundation of China (Grant No. 52008033).

References

1. Nassur AM, Léger D, Lefèvre M, et al. Effects of Aircraft Noise Exposure on Heart Rate during Sleep in the Population Living Near Airports. *Int J Environ Res Public Health* 2019; 16 20190118. DOI: 10.3390/ijerph16020269.
2. Basner M and McGuire S. WHO Environmental Noise Guidelines for the European Region: A Systematic Review on Environmental Noise and Effects on Sleep. *Int J Environ Res Public Health* 2018; 15 20180314. DOI: 10.3390/ijerph15030519.
3. Baudin C, Lefèvre M, Champelovier P, et al. Aircraft Noise and Psychological Ill-Health: The Results of a Cross-Sectional Study in France. *Int J Environ Res Public Health* 2018; 15 20180803. DOI: 10.3390/ijerph15081642.
4. Merino-Martínez R, Heblij SJ, Bergmans DHT, et al. Improving Aircraft Noise Predictions ConsideringFan Rotational Speed. *Journal of Aircraft* 2019; 56: 284-294. DOI: 10.2514/1.C034849.
5. Bertsch L, Snellen M, Enghardt L, et al. Aircraft noise generation and assessment: executive summary. *CEAS Aeronautical Journal* 2019; 10: 3-9. DOI: 10.1007/s13272-019-00384-3.
6. Ingard U. On the Theory and Design of Acoustic Resonators. *The Journal of the Acoustical Society of America* 1953; 25: 1037-1061. DOI: 10.1121/1.1907235.
7. Chanaud RC. Effects Of Geometry On The Resonance Frequency Of Helmholtz Resonators. *Journal of Sound and Vibration* 1994; 178: 337-348. DOI: https://doi.org/10.1006/jsvi.1994.1490.
8. Selamet A, Radavich PM, Dickey NS, et al. Circular concentric Helmholtz resonators. *The Journal of the Acoustical Society of America* 1997; 101: 41-51. DOI: 10.1121/1.417986.
9. Selamet A and Lee I. Helmholtz resonator with extended neck. *The Journal of the Acoustical Society of America* 2003; 113: 1975-1985. DOI: 10.1121/1.1558379.
10. Shi X and Ming Mak C. Helmholtz resonator with a spiral neck. *Applied Acoustics* 2015; 99: 68-71. DOI: https://doi.org/10.1016/j.apacoust.2015.05.012.
11. Cai C, Mak C-M and Shi X. An extended neck versus a spiral neck of the Helmholtz resonator. *Applied Acoustics* 2017; 115: 74-80. DOI: https://doi.org/10.1016/j.apacoust.2016.08.020.
12. Merino-Martinez R, VanDercreek C and Snellen M. Evaluation of advanced acoustic imaging methods for microphone--array measurements in closed--section wind tunnels. *28th AIAA/CEAS Aeroacoustics 2022 Conference*.

13. VanDercreek C, Merino-Martínez R, Sijtsma P, et al. Evaluation of the effect of microphone cavity geometries on acoustic imaging in wind tunnels. *Applied Acoustics* 2021; 181: 108154. DOI: https://doi.org/10.1016/j.apacoust.2021.108154.
14. Ghanadi F, Arjomandi M, Cazzolato B, et al. Understanding of the flow behaviour on a Helmholtz resonator excited by grazing flow. *International Journal of Computational Fluid Dynamics* 2014; 28: 219-231. DOI: 10.1080/10618562.2014.922681.
15. Dai X. Vortex convection in the flow-excited Helmholtz resonator. *Journal of Sound and Vibration* 2016; 370: 82-93. DOI: https://doi.org/10.1016/j.jsv.2016.01.053.
16. Kim; H and Selamet A. Acoustic performance of a Helmholtz resonator with flow. *International Journal of Vehicle Noise and Vibration* 2011; 7: 285-305. DOI: 10.1504/ijvnv.2011.043191.
17. Wu G, Lu Z, Xu X, et al. Numerical investigation of aeroacoustics damping performance of a Helmholtz resonator: Effects of geometry, grazing and bias flow. *Aerospace Science and Technology* 2019; 86: 191-203. DOI: https://doi.org/10.1016/j.ast.2019.01.007.
18. Dastourani H and Bahman-Jahromi I. Evaluation of Aeroacoustic Performance of a Helmholtz Resonator System with Different Resonator Cavity Shapes in the Presence of a Grazing Flow. *Journal of Aerospace Engineering* 2021; 34: 04021061. DOI: doi:10.1061/(ASCE)AS.1943-5525.0001309.
19. Zhao H, Lu Z, Guan Y, et al. Effect of extended necks on transmission loss performances of Helmholtz resonators in presence of a grazing flow. *Aerospace Science and Technology* 2018; 77: 228-234. DOI: https://doi.org/10.1016/j.ast.2018.03.002.
20. Pan W, Xu X, Li J, et al. Acoustic damping performance of coupled Helmholtz resonators with a sharable perforated sidewall in the presence of grazing flow. *Aerospace Science and Technology* 2020; 99: 105573. DOI: https://doi.org/10.1016/j.ast.2019.105573.
21. Xu MB, Selamet A and Kim H. Dual Helmholtz resonator. *Applied Acoustics* 2010; 71: 822-829. DOI: https://doi.org/10.1016/j.apacoust.2010.04.007.
22. Cai C and Mak CM. Acoustic performance of different Helmholtz resonator array configurations. *Applied Acoustics* 2018; 130: 204-209. DOI: https://doi.org/10.1016/j.apacoust.2017.09.026.
23. Kim H and Selamet A. Effect of flow on a dual Helmholtz resonator. *Journal of Mechanical Science and Technology* 2020; 34: 581-588. DOI: 10.1007/s12206-020-0106-7.
24. Ghanadi F, Arjomandi M, Cazzolato B, et al. Interaction of a flow-excited Helmholtz resonator with a grazing turbulent boundary layer. *Experimental Thermal and Fluid Science* 2014; 58: 80-92. DOI: https://doi.org/10.1016/j.expthermflusci.2014.06.016.
25. Spillere A, Cordioli JA and Boden H. On the Effect of Boundary Conditions on Impedance Eduction Results. *23rd AIAA/CEAS Aeroacoustics Conference*.
26. Wu W and Guan Y. Numerical investigation on low-frequency noise damping performances of Helmholtz resonators with an extended neck in presence of a grazing flow. *Journal of Low Frequency Noise, Vibration and Active Control* 2021; 40: 2037-2053. DOI: 10.1177/14613484211020584.